

Directional Emission from Dielectric Leaky-Wave Nanoantennas

M. Peter,¹ A. Hildebrandt,² C. Schlickriede,³ K. Gharib,¹ T. Zentgraf,³ J. Förstner,² and S. Linden^{1,*}

¹University of Bonn, Physikalisches Institut, D-53115, Bonn, Germany

²University of Paderborn, Department of Electrical Engineering, D-33098 Paderborn, Germany

³University of Paderborn, Department of Physics, D-33098, Paderborn, Germany

*linden@physik.uni-bonn.de

An important source of innovation in nanophotonics is the idea to scale down known radio wave technologies to the optical regime. One thoroughly investigated example of this approach are metallic nanoantennas which employ plasmonic resonances to couple localized emitters to selected far-field modes [1–3]. While metals can be treated as perfect conductors in the microwave regime, their response becomes Drude-like at optical frequencies. Thus, plasmonic nanoantennas are inherently lossy [4]. Moreover, their resonant nature requires precise control of the antenna geometry [5]. A promising way to circumvent these problems is the use of broadband nanoantennas made from low-loss dielectric materials [6]. Here, we report on highly directional emission from active dielectric leaky-wave nanoantennas made of Hafnium dioxide. Colloidal semiconductor quantum dots deposited in the nanoantenna feed gap serve as a local light source. The emission patterns of active nanoantennas with different sizes are measured by Fourier imaging. We find for all antenna sizes a highly directional emission, underlining the broadband operation of our design.

Nanoantennas have become valuable elements of the photonics toolbox to control and manipulate light on the nanoscale [1–3]. They allow for an efficient interconversion of localized excitations and propagating electromagnetic waves [7, 8]. In receiving mode, nanoantennas can locally increase the light intensity by several orders of magnitude [4, 9]. This property can be used for the efficient excitation of quantum emitters [10, 11] and to boost nonlinear effects [12–16]. In transmitting mode, coupling of quantum emitters to nanoantennas allows for the control of the emission properties [5, 17–19]. For instance, Curto *et al* [5] reported on a highly directional plasmonic Yagi-Uda antenna. Like their microwave counterparts, nanoantennas can be categorized based on their functional principle into two large groups: (i) resonant antennas and (ii) nonresonant traveling wave antennas. So far, most research has focused on resonant nanoantennas based either on plasmonic resonances in metals [18, 20–22] or on Mie resonances in high-refractive index dielectrics [23–25]. In contrast to this, traveling wave antennas operating at optical frequencies have been studied considerably less. However, there is a growing interest in transferring the traveling wave concept to higher operating frequencies in order to achieve non-resonant broadband operation [6, 26, 27].

Leaky-wave antennas are a subset of traveling wave antennas that emit radiation over the whole length of a non-resonant guiding structure supporting the traveling wave [28]. In the case of a leaky-wave antenna with uniform cross-section, the phase velocity of the guided wave has to be larger than the velocity of light in the medium, into which the wave is radiated. The beam direction θ_{beam} measured from the optical axis can be estimated (see Fig. 1 a) by $\sin(\theta_{\text{beam}}) = \beta/k_g$, where β is the propagation constant of the leaky mode for the given cross-section and k_g the wave number in the medium. The beam direction can be controlled by designing the cross-section of the guiding structure. The finite length of the wave guide as well as the radiation losses give rise to side lobes. The complete radiation pattern in the far field can be obtain by solving the Fraunhofer diffraction integral of the aperture distribution [28].

In this letter, we report on an active, dielectric, leaky-wave antenna for optical frequencies with high directivity. Our antenna design [29] consists of only two

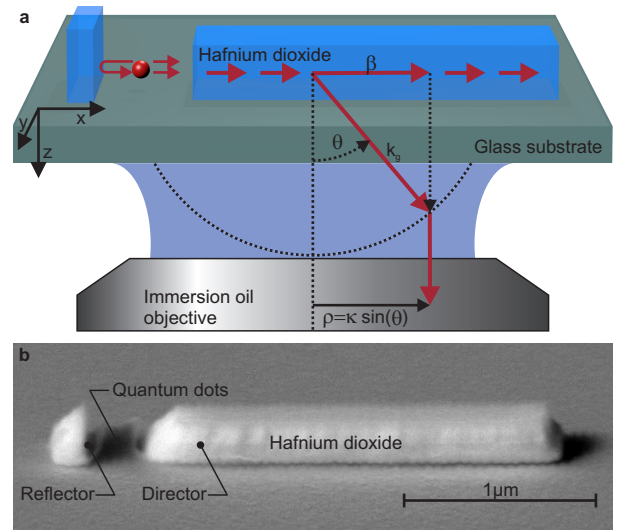


Figure 1: **a** Schematic representation of the operating principle of the dielectric nanoantenna: The fluorescence of the quantum dots excites a leaky mode in the director by end-fire coupling. Light propagating along the director is continuously coupled to radiating modes in the substrate. Emission into the air is prohibited since the phase velocity of the guided wave is smaller than that of light in air. The beam direction is given by $\sin(\theta_{\text{beam}}) = \beta/k_g$, where β is the propagation constant and k_g the wave number of light in the substrate. To increase the gain of the antenna, the reflector redirects fluorescence emitted in the backward direction. The intensity distribution in the back-focal plane of the collecting objective is related to the angular distribution of emitted light by the sine-condition. **b** Scanning electron micrograph of a Hafnium dioxide nanoantenna. Quantum dots (not visible) are deposited into the feed gap between director and reflector.

simple dielectric building blocks and has a total length of approximately three times the free space operation wavelength. The operating principle of the active nanoantenna is shown in Fig. 1a. It can be easily adapted to various low-loss dielectric materials. Moreover, its non-resonant nature makes it inherently robust against fabrication imperfections and guarantees broad-band operation.

The leaky-wave antennas are made of Hafnium diox-

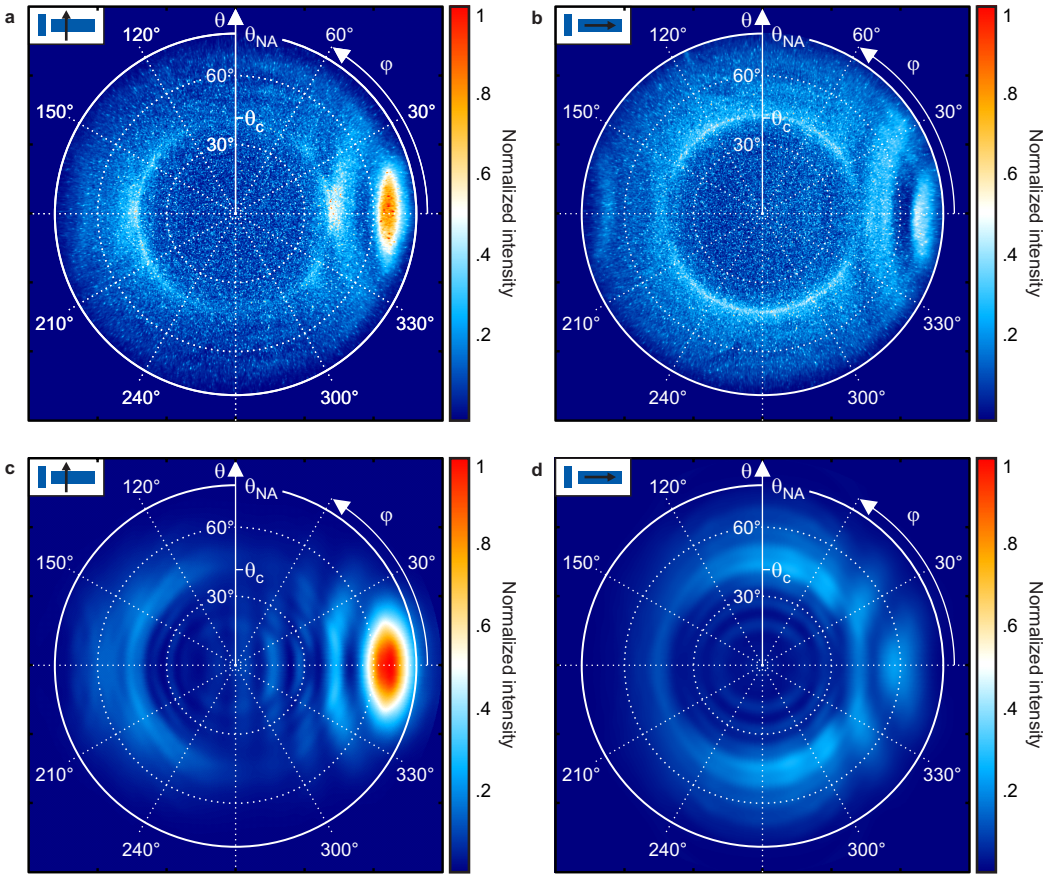


Figure 2: **a** and **b** Measured angular intensity distributions of an active dielectric nanoantenna for two different analyzer settings (see inset) normalized to the same value. The main lobe maxima in both distributions are at $\theta_{\max} = 70^\circ$. The central ring-like feature is attributed to dipoles not coupled to the antenna emitting directly into the substrate. The white circle at $\theta_{NA} = 79^\circ$ marks the experimentally accessible angular range. The calculated intensity distributions for the corresponding analyzer settings in **c** and **d**, show a similar behavior as the experimental data.

ide (HfO_2) and use colloidal semiconductor quantum dots (CdSeTe) as active elements. The fabrication is done by performing electron beam lithography (EBL) on a standard microscope cover glass followed by electron beam evaporation of HfO_2 (see Methods). An electron micrograph of one of our dielectric antennas is shown in Fig. 1b. It consists of two 180 nm thick HfO_2 elements: The reflector has a footprint of $180 \text{ nm} \times 785 \text{ nm}$ and the director of $2200 \text{ nm} \times 600 \text{ nm}$. They are separated by a 260 nm wide feed gap. Colloidal semiconductor quantum dots with an emission wavelength of $\lambda_{\text{QD}} = 780 \text{ nm}$ are precisely deposited from an aqueous solution into the feed gap of the antenna with the help of a second lithography step.

In the optical experiments, a blue pump laser ($\lambda = 450 \text{ nm}$) is focused by a high-numerical-aperture objective ($100\times$ magnification, $\text{NA}=1.49$) through the substrate onto a single antenna to excite the quantum dots in the feed gap. The fluorescence emitted by this active antenna is collected with the same objective. The spatial intensity distribution in the back-focal plane of the objective is related by the sine condition to the angular distribution of emitted light. A lens creates a real image of the back-focal plane on a camera. To investigate the polarization of the antenna signal, we place a linear polarizer as an analyzer in front of the camera. As a postprocessing step, we transform this image of the momentum space to spherical coordinates (θ, φ) , where θ is the polar angle and φ is the azimuthal angle. The coordinate system is chosen such that the

antenna axis points in the $(\theta = 90^\circ, \varphi = 0^\circ)$ direction and the optical axis corresponds to the $(\theta = 0^\circ)$ direction (see Methods).

Figure 2a depicts the normalized angular intensity distribution emitted by the active dielectric nanoantenna shown above. Here, the analyzer axis is set perpendicular to the antenna axis, i.e., we record the emission of a TE-polarized leaky mode (see inset). The active antenna shows a highly directional emission with a strong main lobe at $(\theta_{\max} = 70^\circ, \varphi_{\max} = 0^\circ)$. This lobe has a full width at half maximum of $\Delta\theta_{\max} = (9 \pm 2)^\circ$ and $\Delta\varphi_{\max} = (24 \pm 4)^\circ$. Additional concentric side lobes around the main lobes are visible. A reference measurement (not shown) with a bare quantum dot sample indicates that the weak circular feature at $\theta \approx \theta_c = 41.1^\circ$ can be attributed to uncoupled quantum dots, which preferentially emit at the critical angle between air and glass [30].

The directivity D of an antenna is defined as the ratio of the peak intensity and the intensity averaged over all directions as observed in the far field [31]. The collection angle in our experiment is limited by the NA of the microscope objective, i.e., light emitted by an angle larger than $\theta_{NA} = 79^\circ$ is not detected. As a result, a part of the intensity distribution is cut off. With this restriction in mind, the directivity of the antenna over the measured part of the distribution can be estimated to be $D = 12.5 \text{ dB}$. In order to compare the performance of our antenna with previous works on nanoantennas, we additionally use the

front-to-back ratio (F/B), defined [5] as the intensity ratio between the maximum at $(\theta_{\max}, \varphi_{\max})$ and the opposing point $(\theta_{\max}, \varphi_{\max} + 180^\circ)$, to quantify the directional performance of our active antenna. The F/B value of the dielectric nanoantenna measured here is 12 dB. This value is quite competitive in comparison with plasmonic nanoantennas [5].

The angular intensity distribution for the analyzer axis parallel to the antenna is shown in Fig. 2b. It is normalized to the same value as the data discussed above. The peak intensity as well as the directivity ($D = 9$ dB) are in this case smaller than that recorded for the perpendicular analyzer setting (compare Fig. 2 a and b). A plausible explanation for these observations is that the coupling of the quantum dots to the TM-polarized leaky mode is less efficient. This interpretation is consistent with numerical calculations.

To support our experimental findings, numerical calculations based on finite integration technique (FIT) using CST Microwave Studio were performed [32]. A single dipole in the feed gap served as the active element and three different perpendicular dipole orientations along the coordinate axes (see Fig. 1 a) were assumed in successive calculations. For each dipole orientation, the far-field intensities for the two analyzer settings used in the experiments were evaluated separately. Finally, the intensities of the three dipole-orientations are summed for each analyzer setting. With this procedure, we simulate the ensemble of quantum dots with random dipole orientations as used in the experiment. The calculated intensity distributions for both analyzer settings are shown in Fig. 2c and 2d. They feature the same main and side lobes as the experimental data. The corresponding directivities for the analyzer in the y - and x -direction are $D = 14.05$ dB and in $D = 8.347$ dB, respectively. A detailed analysis of the different dipole orientations shows that there are two main contributions to the main lobes: (i) the dipole oriented along the y -direction couples primarily to the TE leaky mode and (ii) the dipole oriented along the z -direction predominately excites the TM leaky mode. A comparison of these two cases shows that the coupling efficiency to the TM mode is smaller, resulting in a lower directivity for light polarized along the antenna axis.

A main advantage of non-resonant antennas is their high bandwidth and robustness against fabrication imperfections. Hence, we anticipate that the variation of the antenna dimensions will result in a different beam direction but not a total loss of the antenna's functionality. We measured the angular intensity distribution of antennas with footprints $0.8\times$ and $1.4\times$ as large as the original design. The height was not scaled. As anticipated, both antennas still show directional emission (see Fig. 3 a and b). This behavior agrees well with the numerical calculations, which predict a plateau of high directivities for a broad range of the widths and lengths around the original design [29].

In conclusion, we have fabricated and characterized active dielectric nanoantennas for the optical regime. The antennas exhibit highly directional emission. Experiments with different antenna sizes indicate the broadband operation of our nanoantenna design. These characteristics make the active antenna a promising candidate for future applications. We envision that the dielectric antenna in combination with a single quantum emitter may be used

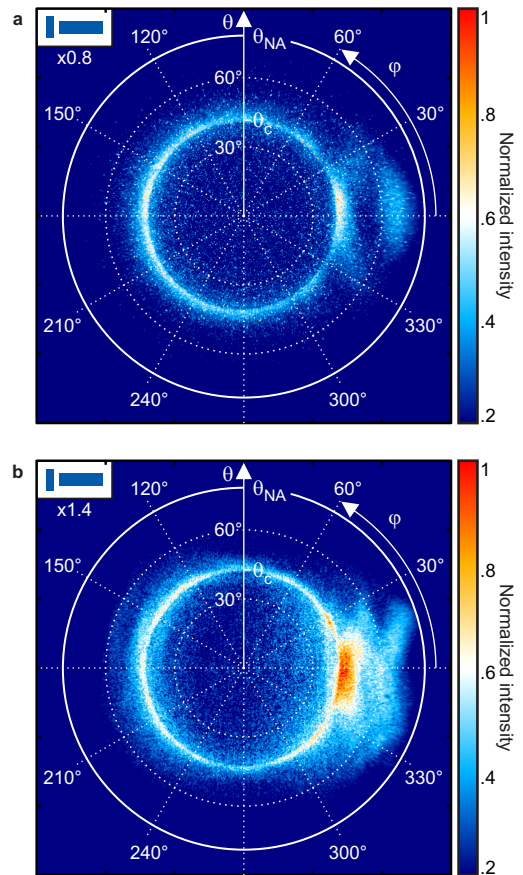


Figure 3: Angular intensity distribution of dielectric antennas without analyzer with footprints (a) $0.8\times$ and (b) $1.4\times$ as large as the original design. The white circle marks the experimentally accessible angular range.

as a highly directional single-photon source without inherent losses. By placing the dielectric antenna into a liquid crystal cell, the beam direction can potentially be tuned electrically.

Methods

Antenna Processing

The sample substrate is a microscope cover glass coated with an 8-nm thick layer of Indium Tin oxide (ITO) to provide sufficient conductivity for the electron beam lithography (EBL) process. As a lithography resist we use a double layer of PMMA spin coated onto the substrate. The sublayers consist of 260 nm PMMA with 600 k molar mass and 200 nm PMMA with 950 k molar mass. The geometries of the antennas are written with a standard EBL system consisting of a Zeiss SIGMA scanning electron microscope equipped with a Raith Beam Controller. A 180 nm thick film of HfO_2 is evaporated by electron-beam evaporation (HVB 100L, Winter Vakuumtechnik). During the deposition the temperature of the sample is kept under 100°C . The PMMA template and the residual HfO_2 is removed in a lift-off process, where the sample is submerged in 60°C N-Methyl-2-pyrrolidone (NMP) for 3.5 h.

Quantum Dot Deposition

We use commercial CdSeTe quantum dots (QDs) that are shelled with ZnS and coated with a polymer providing carboxyl surface groups (Qdot 800 Carboxyl Quantum Dots, Thermo Fisher Scientific). The aqueous QD solution is pH buffered. To deposit the QDs in the antenna feed gap, we use a second lithographic step combined with chemical linking. For this purpose the sample with the HfO₂ antennas is coated again with a PMMA layer. The areas, where QD shall be deposited are defined by exposure with the electron beam. The resolution here is restricted by the proximity effect to approximately 30 nm. After development, the PMMA film with the holes serves as a template for the subsequent surface functionalization. For this purpose, the sample is placed for an hour in a solution of 10 % (3-Aminopropyl)triethoxysilane (APTES) in isopropyl alcohol to silanize the ITO layer in the unveiled patches. Next, 1-Ethyl-3-(3-dimethylaminopropyl) carbodiimide (EDC) is added to the QD solution and the substrate is immersed for two hours with constant stirring in this solution. EDC acts as an activating agent that mediates the link between the carboxyl surface groups of the QDs and the silanized substrate. After rinsing the substrate with deionised water, the PMMA mask is finally removed in a lift-off process and the QDs stick to the modified surface areas.

Optical Setup

A gain switched diode laser ($\lambda = 450$ nm, PiL063X, ALS) is focused through a high numerical aperture microscope objective (CFI Aplanachromat TIRF 100x Oil/1.49/0.12, Nikon) to pump the QDs in the feed gap of a single active nanoantenna. In order to scan an image of the sample and to position the feed gap of the antenna in the focus of the pump light, the sample is mounted on a three axis piezo system (NanoCube XYZ P-611.3S, Physik Instrumente). The fluorescence is separated from reflected pump light by a dichroic mirrors (Beamsplitter T 510LPXRXT, AHF) and a series of optical filters (794/160 BrightLine HC, AHF; FGL550, Thorlabs). The intensity is recorded with a scientific CMOS camera (Zyla, Andor).

Coordinate Transformation

For our aplanatic objective lens, the spatial intensity distribution in the back-focal plane of the objective is related to the angular distribution of the collected light by the sine condition. This distribution is imaged by a lens onto the camera. Thus, an emission angle θ , measured with respect to the optical axis, corresponds to a distance $\rho = \sqrt{x_{\text{cam}}^2 + y_{\text{cam}}^2}$ from the optical image center:

$$\rho = \kappa \sin(\theta) \quad , \quad (1)$$

where κ is the conversion factor. The biggest angle θ_{NA} that can be still collected with the objective and hence be observed on the camera corresponds to the radius of a ring with $\rho_{\text{NA}} = \kappa \text{NA}/n_g$. This relation is used with the known NA to determine the conversion factor κ .

Antenna data is commonly represented in spherical coordinates (θ, φ) , where θ is the polar and φ the azimuthal angle. In our analysis, we choose the orientation such that the antenna axis points in the $(\theta = 90^\circ, \varphi = 0^\circ)$ direction

and the optical axis corresponds to the $(\theta = 0^\circ)$ direction. The data is presented in this letter with a linear θ axis and not in the pseudo momentum space of the camera chip. So, the transformation from the x_{cam} and y_{cam} coordinates of the camera chip to spherical coordinates reads:

$$\theta = \arcsin\left(\frac{\sqrt{x_{\text{cam}}^2 + y_{\text{cam}}^2}}{\kappa}\right), \quad (2)$$

$$\varphi = \arctan\left(\frac{y_{\text{cam}}}{x_{\text{cam}}}\right). \quad (3)$$

Author contributions

M.P. and K.G. conceived and built the optical setup. A.H. developed the antenna design and performed the numerical calculations. M.P. fabricated the samples and established the QD deposition technique. C.S. deposited the dielectric. M.P. performed the measurements and analyzed the data. S.L. and M.P. wrote the manuscript with input from all authors. S.L. supervised the experimental part of the project. J.F. supervised the numerical calculation part of the project. T.Z. supervised the fabrication part of the dielectric antennas.

Acknowledgements

S.L. and M.P. acknowledge financial support through DFG TRR 185 and by the German Federal Ministry of Education and Research through the funding program Photonics Research Germany (project 13N14150). A.H., J.F., and T.Z. acknowledge financial support through DFG TRR 142 and DFG GRK 1464.

Competing financial interests

The authors declare no competing financial interests.

References

- [1] Bharadwaj, P., Deutsch, B. & Novotny, L. Optical Antennas. *Adv. Opt. Photon.* **1**, 438 (2009).
- [2] Novotny, L. & van Hulst, N. Antennas for light. *Nat. Photonics* **5**, 83–90 (2011).
- [3] Eisler, H., Martin, O. J. F., Hecht, B., Mu, P. & Pohl, D. W. Resonant Optical Antennas. *Science* **308**, 1607–1609 (2005).
- [4] Maier, S. A. *Plasmonics: Fundamentals And Applications* (Springer Science & Business Media, New York, 2007).
- [5] Curto, A. G. *et al.* Unidirectional emission of a quantum dot coupled to a nanoantenna. *Science* **329**, 930–933 (2010).
- [6] Monticone, F. & Alù, A. Leaky-wave theory, techniques, and applications: From microwaves to visible frequencies. *Proc. IEEE* **103**, 793–821 (2015).

- [7] Biagioni, P., Huang, J. & Hecht, B. Nanoantennas for visible and infrared radiation. *Rep. Prog. Phys.* **024402**, 76 (2012).
- [8] Taminiau, T., Stefani, F., Segerink, F. & Van Hulst, N. Optical antennas direct single-molecule emission. *Nat. Photonics* **2**, 234–237 (2008).
- [9] Krasnok, A. E. *et al.* Optical nanoantennas. *Phys. Usp.* **56**, 539–564 (2013).
- [10] Pfeiffer, M. *et al.* Enhancing the optical excitation efficiency of a single self-assembled quantum dot with a plasmonic nanoantenna. *Nano Lett.* **10**, 4555–4558 (2010).
- [11] Ureña, E. B. *et al.* Excitation enhancement of a quantum dot coupled to a plasmonic antenna. *Adv. Mater.* **24** (2012).
- [12] Linnenbank, H., Grynko, Y., Förstner, J. & Linden, S. Second harmonic generation spectroscopy on hybrid plasmonic / dielectric nanoantennas. *Light: Sci. Appl.* **5**, 1–7 (2015).
- [13] Metzger, B. *et al.* Strong enhancement of second harmonic emission by plasmonic resonances at the second harmonic wavelength. *Nano Lett.* **15**, 3917–3922 (2015).
- [14] Schumacher, T. *et al.* Nanoantenna-enhanced ultrafast nonlinear spectroscopy of a single gold nanoparticle. *Nat. Commun.* **2**, 333 (2011).
- [15] Wang, H. F. *et al.* In vitro and in vivo two-photon luminescence imaging of single gold nanorods. *Proc. Natl. Acad. Sci. U.S.A.* **102**, 15752–15756 (2005).
- [16] Ghenuche, P., Cherukulappurath, S., Taminiau, T. H., van Hulst, N. F. & Quidant, R. Spectroscopic mode mapping of resonant plasmon nanoantennas. *Phys. Rev. Lett.* **101**, 116805 (2008).
- [17] Kühn, S., Håkanson, U., Rogobete, L. & Sandoghdar, V. Enhancement of single-molecule fluorescence using a gold nanoparticle as an optical nanoantenna. *Phys. Rev. Lett.* **97**, 017402 (2006).
- [18] Hoang, T. B. *et al.* Ultrafast spontaneous emission source using plasmonic nanoantennas. *Nat. Commun.* **6**, 7788 (2015).
- [19] Dregely, D. *et al.* Imaging and steering an optical wireless nanoantenna link. *Nat. Commun.* **5** (2014).
- [20] Farahani, J. N., Pohl, D. W., Eisler, H. J. & Hecht, B. Single quantum dot coupled to a scanning optical antenna: A tunable superemitter. *Phys. Rev. Lett.* **95** (2005).
- [21] Muskens, O. L., Giannini, V., Sánchez-Gil, J. A. & Gómez Rivas, J. Strong enhancement of the radiative decay rate of emitters by single plasmonic nanoantennas. *Nano Lett.* **7**, 2871–2875 (2007).
- [22] Knight, M. W. *et al.* Aluminum Plasmonic Nanoantennas. *Nano Lett.* **12**, 6000–6004 (2012).
- [23] Zhao, Q., Zhou, J., Zhang, F. & Lippens, D. Mie resonance-based dielectric metamaterials. *Mater. Today* **12**, 60–69 (2009).
- [24] Staude, I. *et al.* Tailoring directional scattering through magnetic and electric resonances in subwavelength silicon nanodisks. *ACS Nano* **7**, 7824–7832 (2013).
- [25] Fu, Y. H., Kuznetsov, A. I., Miroshnichenko, A. E., Yu, Y. F. & Luk’yanchuk, B. Directional visible light scattering by silicon nanoparticles. *Nat. Commun.* **4**, 1527 (2013).
- [26] Shegai, T. *et al.* Unidirectional broadband light emission from supported plasmonic nanowires. *Nano Lett.* **11**, 706–711 (2011).
- [27] Esquius-Morote, M., Gomez-Diaz, J. S. & Perruisseau-Carrier, J. Sinusoidally modulated graphene leaky-wave antenna for electronic beamscanning at THz. *IEEE Trans. THz Sci. Technol.* **4**, 116–122 (2014).
- [28] Johnson, R. C. *Antenna Engineering Handbook* (McGraw-Hill, New York, 2007).
- [29] Hildebrandt, A., Reichelt, M., Meier, T. & Förstner, J. Engineering plasmonic and dielectric directional nanoantennas. *SPIE OPTO* **8984**, 89841G (2014).
- [30] Novotny, L. & Hecht, B. *Principles Of Nano-Optics* (Cambridge University Press, Cambridge, 2012).
- [31] Kraus, J. & Marhefka, R. *Antennas For All Applications* (McGraw-Hill, New York, 2002).
- [32] Weiland, T. A discretization model for the solution of maxwell’s equations for six-component fields. *Electron. Commun. AEU* **31**, 116–120 (1977).